Conference Proceedings of the Society for Experimental Mechanics Series

Matthew Allen
Walter D'Ambrogio
Dan Roettgen *Editors*

Dynamic Substructures, Volume 4

Proceedings of the 40th IMAC, A Conference and Exposition on Structural Dynamics 2022

SEM

Springer

Conference Proceedings of the Society for Experimental Mechanics Series

Series Editor
Kristin B. Zimmerman
Society for Experimental Mechanics, Inc.,
Bethel, CT, USA

The Conference Proceedings of the Society for Experimental Mechanics Series presents early findings and case studies from a wide range of fundamental and applied work across the broad range of fields that comprise Experimental Mechanics. Series volumes follow the principle tracks or focus topics featured in each of the Society's two annual conferences: IMAC, A Conference and Exposition on Structural Dynamics, and the Society's Annual Conference & Exposition and will address critical areas of interest to researchers and design engineers working in all areas of Structural Dynamics, Solid Mechanics and Materials Research.

Matthew Allen • Walter D'Ambrogio • Dan Roettgen
Editors

Dynamic Substructures, Volume 4

Proceedings of the 40th IMAC, A Conference and Exposition on Structural Dynamics 2022

Springer

Editors
Matthew Allen
Brigham Young University
Provo, UT, USA

Dan Roettgen
Sandia National Laboratories
Albuquerque, NM, USA

Walter D'Ambrogio
DIIIE
University of L'Aquila
L'AQUILA, L'Aquila, Italy

ISSN 2191-5644 ISSN 2191-5652 (electronic)
Conference Proceedings of the Society for Experimental Mechanics Series
ISBN 978-3-031-04093-1 ISBN 978-3-031-04094-8 (eBook)
https://doi.org/10.1007/978-3-031-04094-8

This Springer imprint is published by the registered company Springer Nature Switzerland AG
The registered company address is: Gewerbestrasse 11, 6330 Cham, Switzerland

Preface

Dynamic Substructures represents one of nine volumes of technical papers presented at the 40th IMAC, A Conference and Exposition on Structural Dynamics, organized by the Society for Experimental Mechanics, and held February 7–10, 2022. The full proceedings also include volumes titled *Nonlinear Structures & Systems*; *Dynamics of Civil Structures*; *Model Validation and Uncertainty Quantification*; *Special Topics in Structural Dynamics & Experimental Techniques*; *Rotating Machinery, Optical Methods & Scanning LDV Methods*; *Sensors and Instrumentation, Aircraft/Aerospace and Dynamic Environments Testing*; *Topics in Modal Analysis & Parameter Identification*; *and Data Science in Engineering*.

Each collection presents early findings from experimental and computational investigations on an important area within structural dynamics. Coupled structures or, substructuring, is one of these areas.

Substructuring is a general paradigm in engineering dynamics where a complicated system is analyzed by considering the dynamic interactions between subcomponents. In numerical simulations, substructuring allows one to reduce the complexity of parts of the system in order to construct a computationally efficient model of the assembled system. A subcomponent model can also be derived experimentally, allowing one to predict the dynamic behavior of an assembly by combining experimentally and/or analytically derived models. This can be advantageous for subcomponents that are expensive or difficult to model analytically. Substructuring can also be used to couple numerical simulation with real-time testing of components. Such approaches are known as hardware-in-the-loop or hybrid testing.

Whether experimental or numerical, all substructuring approaches have a common basis, namely the equilibrium of the substructures under the action of the applied and interface forces and the compatibility of displacements at the interfaces of the subcomponents. Experimental substructuring requires special care in the way the measurements are obtained and processed in order to assure that measurement inaccuracies and noise do not invalidate the results. In numerical approaches, the fundamental quest is the efficient computation of reduced order models describing the substructure's dynamic motion. For hardware-in-the-loop applications, difficulties include the fast computation of the numerical components and the proper sensing and actuation of the hardware component. Recent advances in experimental techniques, sensor/actuator technologies, novel numerical methods, and parallel computing have rekindled interest in substructuring in recent years leading to new insights and improved experimental and analytical techniques.

The organizers would like to thank the authors, presenters, session organizers, and session chairs for their participation in this track.

Provo, UT, USA — Matthew Allen
L'Aquila, Italy — Walter D'Ambrogio
Albuquerque, NM, USA — Dan Roettgen

Contents

Chapter 1
Uncertainty in Power Flow Due to Measurement Errors in Virtual Point Transformation for Frequency-Based Substructuring

Jon Young and Kyle Myers

Abstract Experimental substructuring by means of virtual point transformation (VPT) can be utilized to implicitly account for rotational degrees of freedom (DOFs) at the coupling boundary of a given substructure. Measured frequency response functions (FRFs) are cast onto a "virtual" node containing three translational and three rotational DOFs via a projection matrix, which is determined by geometric relations between impact and response locations on the structure. In this study, the uncertainty of power flow due to measurement errors in the projection matrix and FRFs is quantified by means of Monte-Carlo simulation. This is performed on a numerical model of two beam structures and is then compared to experimentally obtained data using an impact modal test. Upper and lower bounds on the broadband power flow are created using these data. It is shown that closely space modes lead to high variability in the calculation of power flow near resonance even for small measurement errors. Metrics for analyzing the quality of the virtual point transformation are discussed, as well. This work is beneficial to understanding how experimental errors manifest in the calculation of power flow between coupled structures.

Keywords Power flow · Dynamic substructuring · Virtual point transformation · Monte-Carlo · Uncertainty quantification

1.1 Introduction

Frequency-based substructuring has been thoroughly developed over the past several decades for the steady-state analysis of numerical structural models. Its application to experimental data, however, leads to several difficulties which, in general, make experimental substructuring a more cumbersome means of predicting the dynamics of complex structures [1]. A set of frequency response functions (FRFs) are used to define the dynamic properties of the structures of interest when they are uncoupled from each other [2–4]. These FRFs are then assembled by enforcing displacement compatibility and force equilibrium on their coupling interfaces, and the resulting FRFs predict the frequency response of the assembled structures. These FRFs are generally obtained using modal impact testing, but shakers or laser vibrometers can also be used [5]. Of course, measurement errors due to noise and uncertainty in the exact position and orientation of accelerometers and impacts are inevitable, but the measurements of rotational degrees of freedom (DOFs) which contain necessary information for proper substructure coupling are generally impossible to measure. Moreover, these errors are drastically amplified during substructure assembly due to the inversion of the interface FRFs and further magnified if power flow between substructures is calculated due to its quadratic form.

To account for the rotational DOFs on the substructure interfaces, the virtual point transformation (VPT) has been developed and successfully used to couple experimental substructures [6–8]. It implements a least-squares residual minimization to project the dynamics measured by accelerometers onto a virtual point which contains three translational and three rotational DOFs. The projection is done using only the geometric relations between the virtual point and the interface impact and response measurements. The primary assumption is that the interface being modelled with a virtual point behaves rigidly in the frequency range being analyzed. That is, there is no local flexible deformation of the interface.

J. Young (✉)
Department of Mechanical Engineering, Pennsylvania State University, State College, PA, USA

K. Myers
Structural Acoustics Department, Penn State Applied Research Laboratory, State College, PA, USA
e-mail: krm25@arl.psu.edu

M. Allen et al. (eds.), *Dynamic Substructures, Volume 4*, Conference Proceedings of the Society for Experimental Mechanics Series,
https://doi.org/10.1007/978-3-031-04094-8_1

Metrics such as overall sensor and impact consistency have been developed to quantify this assumption for a given virtual point [9].

The VPT has been developed to be applied to the Lagrange Multiplier Frequency-Based Substructuring (LMFBS) method [3]. It is known as a dual substructure assembly method because in addition to the displacements of the assembled structure being solved for, the coupling force between substructure interfaces is explicitly solved for. This is particularly useful when calculating power flow because it can be expressed in terms of the coupling interface mobility and the coupling force between substructures. Power flow between substructures through flexible joints has been studied in the past using the LMFBS as the method of assembly [10]. However, this study focused on correcting a numerical model with a flexible elastic and dissipative interface so the response of the assembly would better match experimental data. This type of interface modelling will not be used in this work, and instead a rigid connection is assumed.

Since the VPT requires the projection of physical measurements onto a virtual node near the coupling interface of a substructure, it would be beneficial to know how measurement errors in this projection propagate through the calculation of a response quantity. In this study, power flow from a source to receiver beam structure is the response quantity of interest because it is a single scalar measure of the response of the assembled structures. Measurement uncertainty in both the projection matrix and FRFs is tracked through the substructure assembly process and calculation of power flow, and distributions of power flow and overall sensor consistency are estimated using the results from a Monte-Carlo simulation. Additionally, different ranges of maximum uncertainty in the projection matrix measurements are studied to understand how variability in power flow changes with respect to the amount of uncertainty in the VPT. These simulated results are then compared to some preliminary experimental data.

1.2 Virtual Point Transformation

The VPT projects measured displacements and forces onto a virtual point with three translational and three rotational DOFs. The projection of the response measured by accelerometer k onto virtual point v is given by

$$\mathbf{u}^k = \mathbf{R}_{\mathbf{u}}^{kv}\mathbf{q}^v + \boldsymbol{\mu}^k \tag{1.1}$$

where

$$\mathbf{R}_{\mathbf{u}}^{kv} = \begin{bmatrix} e_{x,X}^k & e_{x,Y}^k & e_{x,Z}^k \\ e_{y,X}^k & e_{y,Y}^k & e_{y,Z}^k \\ e_{z,X}^k & e_{z,Y}^k & e_{z,Z}^k \end{bmatrix} \begin{bmatrix} 1 & 0 & 0 & 0 & r_Z^k & -r_Y^k \\ 0 & 1 & 0 & -r_Z^k & 0 & r_X^k \\ 0 & 0 & 1 & r_Y^k & -r_X^k & 0 \end{bmatrix} \tag{1.2}$$

is the displacement projection matrix. In previous literature, this matrix is said to contain the *interface deformation modes*. The vector $\mathbf{u}^k$ are the physical displacements measured by accelerometer k, and the vector $\mathbf{q}^v$ are the virtual point displacements of virtual point v. This vector contains three translational and three rotational DOFs. Since the VPT assumes a locally rigid interface, the vector μ^k contains the residual flexible motion of the interface measured by accelerometer k. The left matrix in Eq. 1.2 corresponds to the orientation of the accelerometer in the virtual point coordinate system, and the right matrix contains the projection information for the translational and rotational DOFs of the virtual point. A similar projection is performed for the interface forces applied to the structure

$$\mathbf{m}^v = \mathbf{R}_{\mathbf{f}}^{vh} \left\| \mathbf{f}^h \right\| \tag{1.3}$$

where

$$\mathbf{R}_{\mathbf{f}}^{hv} = \left\{ e_X^h \; e_Y^h \; e_Z^h \right\} \begin{bmatrix} 1 & 0 & 0 & 0 & r_Z^h & -r_Y^h \\ 0 & 1 & 0 & -r_Z^h & 0 & r_X^h \\ 0 & 0 & 1 & r_Y^h & -r_X^h & 0 \end{bmatrix} \tag{1.4}$$

is the force projection matrix. Note that the transpose of the force projection matrix is given in Eq. 1.3 due to the virtual point moments not being able to be uniquely defined given only impact force magnitude $\|\mathbf{f}^h\|$ and orientation. Here, $\mathbf{m}^v$ are the virtual forces on virtual point v, and $\mathbf{f}^h$ is the force vector of interface impact h whose direction is given by $\left\{ e_X^h \; e_Y^h \; e_Z^h \right\}$.

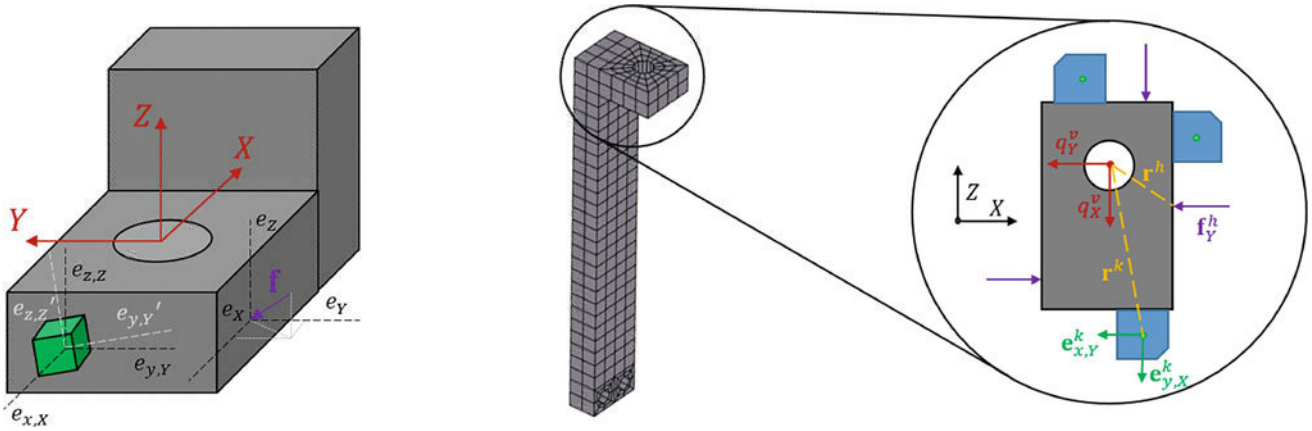

Fig. 1.1 Perturbations in FRFs considered with accelerometer in green and applied interface impact in purple (left); VPT coordinate system and quantities needed to construct projection matrices (right)

In Eq. 1.2, $e_{c,D}^k$ and r_D^k are the local direction and distance vectors for accelerometer k, respectively. That is, $e_{c,D}^k$ is the local direction c of accelerometer k expressed in the virtual point coordinate direction D of virtual point v. Additionally, in Eq. 1.4, e_D^h and r_D^h are the direction and distance vectors for applied force h. Since impact forces are only measured in a single direction, as compared to a tri-axial accelerometer which measures the response in three orthogonal directions, there is no local coordinate system associated with the applied force. Its direction is simply expressed in the virtual point coordinate system.

Geometric relations between both the interface displacements and forces are given in Fig. 1.1 (right). The VPT is performed by determining a transformation matrix which relates the physical and virtual coordinates. This is done in a least-squares sense using the pseudo-inverse giving

$$\mathbf{q} = \left(\mathbf{R}_\mathbf{u}^T \mathbf{R}_\mathbf{u}\right)^{-1} \mathbf{R}_\mathbf{u}^T \mathbf{u} = \mathbf{T}_\mathbf{u} \mathbf{u} \tag{1.5}$$

$$\mathbf{f} = \left(\mathbf{R}_\mathbf{f} \mathbf{R}_\mathbf{f}^T\right)^{-1} \mathbf{R}_\mathbf{f} \mathbf{m} = \mathbf{T}_\mathbf{f}^T \mathbf{m} \tag{1.6}$$

These transformations can then be applied to the LMFBS to calculate the virtual point displacements. Doing so gives

$$\mathbf{q}_{\text{ass}} = \mathbf{T}_\mathbf{u} \mathbf{Y} \mathbf{T}_\mathbf{f}^T \left(\mathbf{f} - \mathbf{B}_\mathbf{f}^T \boldsymbol{\lambda}\right) \tag{1.7}$$

where $\mathbf{q}_{\text{ass}}$ contains the virtual point displacements of the assembled structures and

$$\boldsymbol{\lambda} = \left(\mathbf{B}_\mathbf{u} \mathbf{T}_\mathbf{u} \mathbf{Y} \mathbf{T}_\mathbf{f}^T \mathbf{B}_\mathbf{f}^T\right)^{-1} \mathbf{B}_\mathbf{u} \mathbf{T}_\mathbf{u} \mathbf{Y} \mathbf{f} \tag{1.8}$$

is the coupling force between the virtual point connections. This quantity is used to calculate power flow. The matrices $\mathbf{B}_\mathbf{u}$ and $\mathbf{B}_\mathbf{f}$ identify the virtual point partition of the FRFs in the event that internal DOFs on either the source or receiver are retained, and $\mathbf{Y}$ is a block diagonal matrix containing the source and receiver FRFs. Power can then be calculated using

$$P = \tfrac{1}{2} \operatorname{Re}\left\{\boldsymbol{\lambda}^H \mathbf{Y}_{vv}^{(r)} \boldsymbol{\lambda}\right\} \tag{1.9}$$

where the subscript vv indicates the virtual point FRF partition and the superscript (r) indicates a quantity pertaining to the receiver beam. The response of this quantity to measurement uncertainty in the projection matrices is what is to be studied via Monte-Carlo simulation.

1.3 Numerical Methods

A sampling size of 100,000 power flow calculations was used in the Monte-Carlo simulation over a frequency spectrum ranging from 60 to 6000 Hz, increasing in increments of 1 Hz. Four different test cases were simulated:

1. Perturb only r_D^k and r_D^h of the projection matrices, with maximum measurement uncertainty (error) ranging from $\pm 0.05''$ to $\pm 0.45''$, increasing in increments of $0.1''$.
2. Perturb only the values of $e_{c,D}^k$, e_D^h, r_D^k, and r_D^h of the projection matrices, whose ranges are specified in Table 1.1.
3. Perturb only the angles of the impact forces and accelerometers on the interface (effectively perturbing the FRFs) whose ranges are specified in Table 1.1.
4. Perturb both the projection matrices and the FRFs in the same manner specified in the previous two cases.

Case 3 is shown in Fig. 1.1 (left). The 100,000 power flows calculated at a given frequency was allocated to 1 of the 120 bins ranging from the maximum to minimum power flow calculated at that frequency. The distribution of overall sensor consistency was determined in this way as well. Overall sensor consistency was calculated by applying a force to the uncoupled source and receiver sufficiently far from the interface and averaging the source and receiver consistencies as

$$\rho_{\text{avg}} = \tfrac{1}{2}\left(\rho^{(s)} + \rho^{(r)}\right) \tag{1.10}$$

where the overall sensor consistency of interface displacements is given by

$$\rho = \frac{\|\mathbf{R_u q}\|}{\|\mathbf{u}\|} \tag{1.11}$$

which is a measure of how rigid the interface is and therefore how accurate the VPT is in representing the interface dynamics. It is dimensionless and bounded between 0 and 1. Flexible interfaces will have a sensor consistency close to 0, and rigid interfaces will have a consistency close to 1. Perfectly rigid interfaces have a consistency of exactly 1.

In order to determine if the VPT applied to the numerical model accurately represented the dynamics of the assembled source and receiver beams in a numerical setting, a modal analysis of the assembled finite element models was performed in NASTRAN. The two beams were connected using a rigid body element (RBE2 in NASTRAN) to simulate the virtual point connection. It was verified that the first 16 natural frequencies of the assembled structures using the VPT were within 0.025% of the natural frequencies predicted by coupling the structures with the RBE2 (Fig. 1.2).

Due to the measurement uncertainties simulated, it is possible to calculate negative power flows using Eq. 1.9. However, values of power flow below −240 dB were truncated from the data set as negative values cannot be shown on a logarithmic

Table 1.1 Maximum and minimum uncertainties in projection matrix and FRFs for Cases 2–4 of Monte-Carlo simulation

	Projection Matrix				FRFs	
	Accel.		Force			
	Location (in)	Angle (deg)	Location (in)	Angle (deg)	Accel. Angle (deg)	Force. Angle (deg)
Min	−0.25	−2	−0.25	−2	−2	−10
Max	0.25	2	0.25	2	2	10

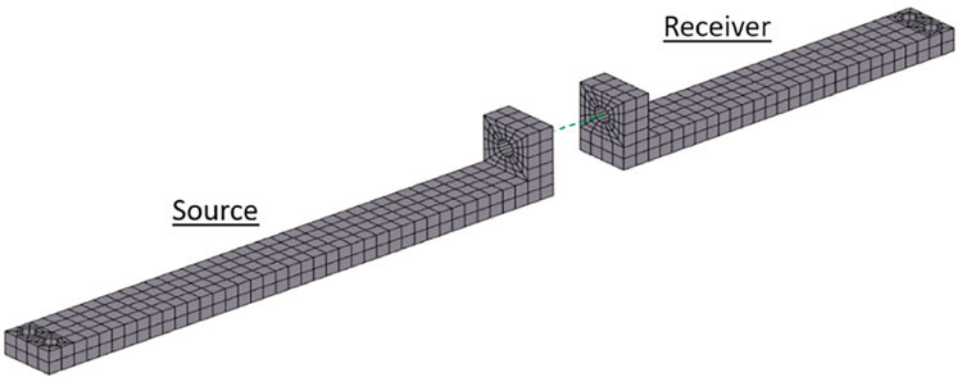

Fig. 1.2 Numerical model of source and receiver beam structures to be coupled using VPT using a single virtual point

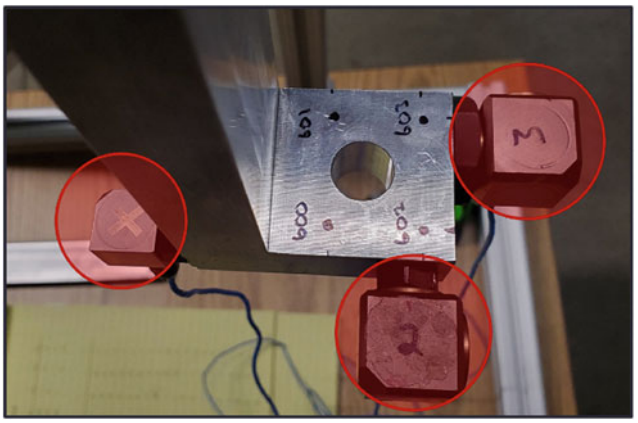

Fig. 1.3 Experimental interface measurements showing three tri-axial accelerometers (highlighted in red) and several impact locations indicated by the points labeled 600–603

scale. Negative power flows will be discussed with the results from Monte-Carlo simulation and the calculation of power flow using experimental data.

1.4 Experimental Methods

Power flow was estimated using experimental data by measuring the response of the uncoupled source and receiver interfaces using three tri-axial accelerometers (two PCB-B07 and one PCB-A14 due to equipment limitations), shown in Fig. 1.3. A total of 15 impacts were made to each interface which were to be projected onto the virtual point. An impact modal hammer (model PCB-086C01) with a metal tip was used to measure the force applied to the interface. A sampling rate of 1 Hz was used at frequencies ranging from 60 to 1600 Hz. This range was sufficient to capture five modes of the assembled substructures predicted by the numerical model, excluding rigid body modes.

Due to their size, it should be mentioned that the mass loading of accelerometers was included in the numerical model described in the previous section. The two PCB-B07 accelerometers weighed approximately 35 g each, and the one PCB-A14 accelerometer weighed 12 g. It will be seen in the results that the mass of the accelerometers on the interface played a much more prominent role in predicting the assembled response of the structure than could be modelled by simply attaching point masses to the interface of the numerical model.

1.5 Results

The effect of measurement uncertainty in the distance parameters in the VPT is shown in Fig. 1.4 at several frequencies. Practically speaking, large variability in power flow can occur due to relatively small errors present when measuring the distance between the virtual point, force, and accelerometer locations in an experimental setup. The distribution of power flow for different ranges of measurement uncertainty is shown at 850 Hz in Fig. 1.4 (left) – effectively Case 1 of the simulation. It can be seen that the statistical mean, media, mode, and standard deviation of power flow change as a function of the uncertainty in the distance parameters of the projection matrices. Additionally, the distribution of power flow in Fig. 1.4 is not Gaussian. The shape of the distribution was heavily dependent on frequency, and while at some frequencies it was heavily skewed to the left or right, at other frequencies, it was approximately Gaussian. Large changes in the distribution of power flow occurred near resonance, but a description of the distribution as a function of frequency has not been developed.

The standard deviation of the power flow distributions is shown at several frequencies in Fig. 1.4 (right). The first frequency (475 Hz) coincides with the second resonant frequency of the assembled system, the second frequency (850 Hz) is between the third and fourth resonant frequencies, the third frequency (2.6 kHz) is near two closely spaced modes, and the fourth frequency (5.5 kHz) is in a frequency region with decreased sensor consistency. The first, second, and fourth frequencies are directly proportional to the measurement uncertainty in the projection matrix distance parameters. The third frequency, near two closely spaced modes, has the highest standard deviation when the maximum measurement uncertainty